Energy Reports 8 (2022) 81–98

Contents lists available at ScienceDirect

Energy Reports

journal homepage: www.elsevier.com/locate/egyr

Research paper

ANT-colony optimization-direct torque control for a doubly fed induction motor : An experimental validation

Said Mahfoud [a], Aziz Derouich [a], Atif Iqbal [b,*], Najib El Ouanjli [a,c]

[a] Industrial Technologies and Services Laboratory, Higher School of Technology, Sidi Mohamed Ben Abdellah University, Fez, Morocco
[b] Department of Electrical Engineering, Qatar University, Doha, Qatar
[c] Faculty of Sciences and Technology, Hassan First University, Settat, Morocco

ARTICLE INFO

Article history:
Received 26 September 2021
Received in revised form 7 November 2021
Accepted 16 November 2021
Available online xxxx

Keywords:
ACO-DTC
dSPACE
ControlDesk
DFIM
Cost functions

ABSTRACT

Direct Torque Control (DTC) presents an optimal solution to control the behaviors of the alternative motors, compared to other controls, because of several advantages offered by this technique, the speed overshoots, fluxes, and torque ripples remain the major factors which minimize the DTC robustness. The regulation speed in DTC is carried out by the classic Proportional Integrator Derivative (PID), which is known for its higher robustness in linear systems, except that in the case of non-linear systems, the PID controller gives poor reactions to variations in the system's parameters. The best solutions adopted in this situation are often based on optimization algorithms that generate the controller's gains in each period where there is an internal or external perturbation, adapting the behaviors of the PID against the system's nonlinearity. For that reason, this work is focused on the theoretical studies and experimental validation on dSPACE Board DS1104 of the new proposed approach based on PID speed regulation, optimized by the Ant Colony Optimization algorithm (ACO) for DTC, applied to both sides of the Doubly Fed Induction Motor (DFIM), to overcome the previous drawbacks cited at the beginning. The new combined ACO-DTC strategy has been studied for optimizing the gains of the PID controller by using a cost function such as Integral Square Error (ISE). The proposed approach is implemented on Matlab/Simulink to validate the objectives adopted by this strategy. The simulation and experimental results extracted from Matlab and ControlDesk have proved the efficiency of the proposed ACO-DTC with the system's nonlinearity, which attribute different enhancements in the global system performance.

1. Introduction

Variable speed drives have gained considerable importance in industry and research in the last decade, and require multidisciplinary knowledge in the field of electrical engineering, such as electrical machines, power electronics, computer science, programmable technologies, and control theory of dynamic systems. Recent developments in these disciplines have made it possible to develop very high-performance control systems. Thus, a variable speed drive consists of an electrical energy source, a power electronics converter, a machine, and a control system (Mahfoud et al., 2021b).

AC machines are used much more in high power applications, such as rolling and railway electric traction (El Ouanjli et al., 2019a; Mahfoud et al., 2021a). Among these types of machines, the most used is the Doubly Fed Induction Motor (DFIM), which has a wound rotor, that has been developed to effectively maintain the control of the machine and increase the flexibility of the asynchronous machine (Kumar et al., 2019), up to a rotating machine at a speed that can reach twice the asynchronous cage machine (Overspeed) (Mahfoud et al., 2021c; El Ouanjli et al., 2019b). This new development path helps researchers find new controls guaranteeing very good robustness despite the variation in parameters such as resistances and inductances of the stator and rotor, and the impossibility of the immediate estimation of the flux and the rotor currents (El Ouanjli et al., 2019b).

In the field of controls, different approaches are used, which have advantages but are limited by some disadvantages, among these popular controls which are applied on DFIM are the Field Oriented Control (FOC) (Blaschke, 1972; Hasse, 1968), its operating principle is to bring back the behavior of the DFIM similar to a DC machine, to ensure the decoupling between flux and torque (El Ouanjli et al., 2019a; Drid et al., 2005), but this technique requires a sensor positioned in the air gap to directly measure the flux in the case of Direct Field Oriented Control

* Corresponding author at: Department of Electrical Engineering, Qatar University, Doha, Qatar.
E-mail addresses: said.mahfoud@usmba.ac.ma (S. Mahfoud), atif.iqbal@qu.edu.qa (A. Iqbal).

https://doi.org/10.1016/j.egyr.2021.11.239

(DFOC) (Drid et al., 2005), the sensors are subject to physical and mechanical constraints (temperature, vibration) (Mahfoud et al., 2021a), the Indirect Field Oriented Control (IFOC) eliminates the need to use a sensor of the flux, the major disadvantage of this method is the sensibility of the estimation in towards the variation of the machine parameters (Amezquita-Brooks et al., 2015), especially the stator and rotor time constants so the regulation in this control is carried out by six classical PID regulators which make the control very sensitive to the parametrical variations. In Abderazak and Farid (2016) the authors have developed the sliding mode control which is known by the phenomenon of chattering which causes very frequent oscillations affecting the operation and performance of the system (Mazen Alhato et al., 2020).

On the other hand, Takahashi, Noguchi, and Depenbrock (Takahashi and Ohmori, 1989) have evolved the Direct Torque Control (DTC), which makes the behavior of the machine similar to that of the DC machine. The speed regulation of the DTC is controlled by a single classical Proportional Integrator (PI) controller, which makes the DTC control less sensitive to the parametric variation of the machine. This gives the DTC control important robustness compared to the previous ones (Takahashi and Noguchi, 1997), but it introduces important flux and torque ripples (Mahfoud et al., 2021a). For this reason, several approaches have been proposed to limit torque and flux ripples.

In the control of non-linear systems or systems with variable parameters, classical control laws such as PID controllers may be insufficient due to their sensitivity to parameter variations, and they are not robust, especially in cases where precision and other dynamic performances are required (Depenbrock, 1987). For this reason, robust control laws based on artificial intelligence are used, which are insensitive to system parameter variations, internal and external disturbances, and nonlinearities (Jayachitra and Vinodha, 2014).

Detailed studies in the literature are available, which allow PID controllers to be robust in the nonlinear case by optimizing the gains at each period to adapt the system with instantaneous variation. The application of optimization algorithms has become an optimal solution and essential to increase the robustness of a multidisciplinary system. The use of Ant Colony Optimization (ACO) meets the non-linear needs of different systems. The literature proves that ACO represents an ideal solution when compared to other optimization algorithms. In Devasahayam and Veluchamy (2017), the authors used ACO and Particle swarm optimization (PSO) in the identification and rectification of defects in transport electric lines. The authors discovered that the ACO algorithm is more efficient and faster for fault detection and intervention in the injection of reactive power into the transport electric lines. In Herlambang et al. (2019), Herlambang, T., Rahmalia, D., and Yulianto used ACO and PSO to optimize the gains of the PID controller in autonomous underwater vehicles. Oshaba et al. (2017) Oshaba, AS, Ali, ES, and Abd Elazim conducted a comparative study of ACO and Genetic Algorithm (AG) for the optimization of the gains of the speed controller of an Induction Motor (IM) powered by a photovoltaic system and concluded that ACO was more efficient in terms of speed, precision, and stability. In Ram et al. (2021), Ram, SS, Kumar, C., Madhumitha, J., and Nandhini designed fuzzy rules and the ACO to optimize the gains of the PID regulator in order to control the fermenter system's concentration. It turns out that ACO gives better results compared to the fuzzy logic controller. George et al. (2021) George, MA, Kamat, DV, & Kurian have found that the ACO-optimized Fractional Order Proportional Integrator Derivator (FOPID) controller provides optimal speed tracking performance compared to GA and PSO-based fuzzy FOPID controllers in electric vehicles. Mughees and Mohsin (2020) Mughees, A., & Mohsin, concluded that ACO increased the efficiency and stability of the system compared to the Ziegler Nicholas (ZN), GA, PSO, and Evolutionary Programming (EP) method for the control of a Magnetic Levitation SystemIn Das et al. (2015), Madadi and Motlagh (2014) and Kanojiya and Meshram (2012) designed a PID controller for an adopted second-order DC motor system and used Grey wolf optimization (GWO) and PSO algorithms to optimize the PID controller. Hultmann and do Santos (Ayala and dos Santos Coelho, 2012), developed a multi-objective non-dominated sorting GA for tuning a PID controller applied to a robotic manipulator. Krohling and Rey (2001) present a GA-based PID controller for solving the constrained optimization problem in a servo system. The authors discovered in Nagaraj and Murugananth (2010) that ACO-based optimization produces very interesting results in terms of performance, such as response time and stability. In Zemmit et al. (2018), the authors applied a new control strategy for DFIM by optimizing the parameters of the PID speed controller by the genetic algorithm of DTC control applied to the stator, and the rotor was supplied with 12 V voltage and 5 Hz frequency, so as not to have mediocre torque ripples. But under these conditions, the DFIM behaves like an Asynchronous Motor, which does not allow us to take advantage of the benefits offered by DFIM (Overspeed) (BonnetFrancois et al., 2007). In Mahfoud et al. (2021a), the authors applied the same technique used by Zemmit et al. (2018), but this technique is applied to both sides of the DFIM to benefit from all the advantages offered by this machine. Currently, there are three works in the literature that apply optimization algorithms to DTC control of a DFIM, such as Mahfoud et al. (2021a,c) and Zemmit et al. (2018) that use GA for PID controller optimization; in this study, and for the first time in the literature, ACO is used in the DTC of a DFIM. ACO has several advantages, including the ability to have a faster speed response time and a zero static error.

After a brief history in the literature and to improve the scientific and technical research, this article is devoted to the improvement of DTC control performance by optimization algorithm. In this control, the PI speed controller is replaced by a PID controller, whose gains are optimized by the ACO algorithm. In this situation, the new ACO-PID structure adapts to the parametric variation of the machine, generating each time according to the situation of the system the new gains which are supposed to be optimal. The structure of the proposed combined algorithm and control ACO-DTC is presented in the following Fig. 1.

The organizational structure of this paper is adopted by the following sections: Sections 2 and 3 focus on the establishment of the DFIM and DTC models in the α, β-plane. Sections 4 and 5 on the description of the new ACO-DTC control strategy and simulation of the ACO-DTC control on Matlab/Simulink, and Section 6 on the implementation of the proposed ACO-DTC strategy on the dSPACE DS1104 board. Finally, we finish our article by conclusion with a proposal for the planned research work to be done in the future.

2. DFIM Model

By ignoring the core loss of DFIM, the slot effect, the saturation, and so on. In a stationary reference frame, the mathematical model can be deduced from the three-phase model by passing to the Concordia hypotheses, the DFIM model is expressed by equations as follows (El Ouanjli et al., 2019a; Mahfoud et al., 2021a; Kumar et al., 2019):

- Stator Electric equations:

$$\begin{cases} v_{s\alpha} = R_s.i_{s\alpha} + \frac{d\psi_{s\alpha}}{dt} \\ v_{s\beta} = R_s.i_{s\beta} + \frac{d\psi_{s\beta}}{dt} \end{cases} \quad (1)$$

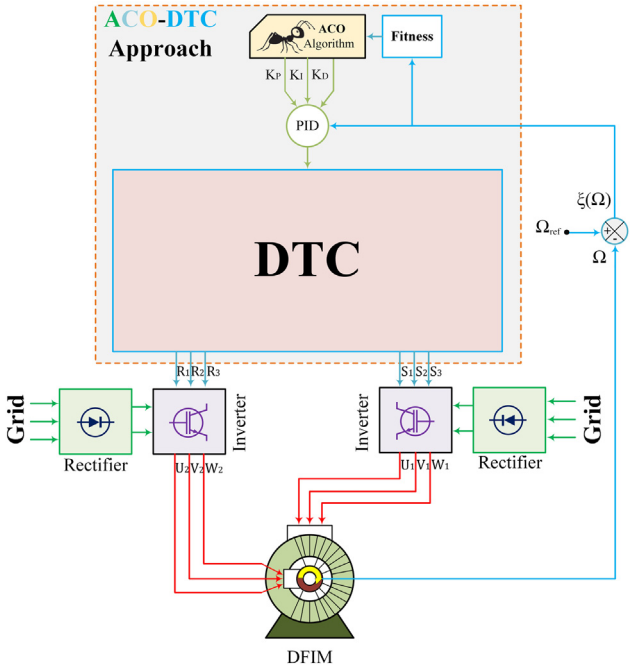

Fig. 1. Proposal structure of DTC based on ACO algorithm for DFIM.

- Rotor Electric equations:

$$\begin{cases} v_{r\alpha} = R_r.i_{s\alpha} + \frac{d\psi_{r\alpha}}{dt} + \omega_m.\psi_{r\beta} \\ v_{r\beta} = R_r.i_{r\beta} + \frac{d\psi_{r\beta}}{dt} - \omega_m.\psi_{r\alpha} \end{cases} \quad (2)$$

- Stator Magnetic equations:

$$\begin{cases} \psi_{s\alpha} = L_s.i_{s\alpha} + L_m.i_{r\alpha} \\ \psi_{s\beta} = L_s.i_{s\beta} + L_m.i_{r\beta} \end{cases} \quad (3)$$

- Rotor Magnetic equations:

$$\begin{cases} \psi_{r\alpha} = L_r.i_{r\alpha} + L_m.i_{s\alpha} \\ \psi_{r\beta} = L_r.i_{r\beta} + L_m.i_{s\beta} \end{cases} \quad (4)$$

- Mechanical equations

$$\begin{cases} T_{em} = p.(\psi_{s\alpha}i_{s\beta} - \psi_{s\beta}i_{s\alpha}) \\ j\frac{d\Omega}{dt} + f\Omega = T_{em} - T_r \end{cases} \quad (5)$$

3. DTC model

3.1. Operating principle

DTC is a motor control method distinct from FOC. I. Takahashi proposed it in the mid-1980s (Mahfoud et al., 2021a). DTC uses hysteresis controllers to estimate the stator flux and electromagnetic torque space vectors and evaluate their amplitude independently and individually (Mahfoud et al., 2021a; Kumar et al., 2019). The hysteresis controllers' outputs are used to select a voltage vector for the Voltage Source Inverter (VSI). It keeps the torque and flux vectors in two hysteresis bands (Mahfoud et al., 2021a). Current controllers are unnecessary in DTC. The DTC in the stator reference framework does not implement coordinate transformation. Direct control of torque and flux eliminates the need for a Pulse Width Modulation (PWM) modulator (Merzoug, 2008; El Ouanjli et al., 2017). It is faster and has a higher dynamic torque response than FOC (El Ouanjli et al., 2019a; Mahfoud et al., 2021a; Kumar et al., 2019). Torque and Flux Estimation.

to simplify the mathematical study of equations which are carried on three axes (I_a, I_b, I_c), the use of the Concordia transform allows us to convert the equations on two axes (I_α, I_β) into reference frames (α, β).

$$I_\alpha = I_a \quad (6)$$

$$I_\beta = \frac{\sqrt{3}}{3}(I_a + 2I_b) \quad (7)$$

Additionally, the DC bus voltage (V_{dc}) is converted and measured to a two-phase reference frame; when combined with the final vector applied to the VSI (S_a, S_b, S_c), the two-phase (V_α, V_β) reference components are as follows:

$$V_\alpha = \frac{V_{DC}}{3}(2.S_a - S_b - S_c) \quad (8)$$

$$V_\beta = \frac{\sqrt{3}V_{DC}}{3}(S_b - S_c) \quad (9)$$

To estimate the stator and rotor magnetic fluxes vectors (ψ_s and ψ_r), the following expression is applied using stator and rotor resistances, voltage, and current (R_s, R_r, V_s, V_r, I_s and I_r) as:

$$\psi_s = \int (V_s - R_s.I_s)\,dt \quad (10)$$

$$\psi_r = \int (V_r - R_r.I_r)\,dt \quad (11)$$

As a result of the flux components estimated in (12) and (13) above, the full range of the stator and rotor fluxes vectors will be as follows:

$$|\psi_s| = \sqrt{\psi_{s\alpha}^2 + \psi_{s\beta}^2} \quad (12)$$

$$|\psi_r| = \sqrt{\psi_{r\alpha}^2 + \psi_{r\beta}^2} \quad (13)$$

Additionally, the angle between the fluxes vectors can be determined using the following expression:

$$\theta_s = \tan^{-1}\frac{\psi_{s\beta}}{\psi_{s\alpha}} \quad (14)$$

$$\theta_r = \tan^{-1}\frac{\psi_{r\beta}}{\psi_{r\alpha}} \quad (15)$$

By including the flux. The electromagnetic torque can be calculated using the following expression:

$$T_{em} = p.(\psi_{s\alpha}.i_{s\beta} - \psi_{s\beta}.i_{s\alpha}) \quad (16)$$

Torque error $\xi(T)$ and flux error $\xi(\psi)$ are calculated by comparing torque and fluxes estimates to their corresponding reference values. Hysteresis comparators will use these error values as input.

3.2. Hysteresis comparators

Fluxes are maintained in a circular crown, this function is performed by two hysteresis comparators with two levels (Fig. 2, a). In addition, a three-level hysteresis comparator controls the electromagnetic torque of the motor in both directions of rotation, producing either positive or negative torque. (Fig. 2, b) shows a three-level hysteresis torque comparator (see Fig. 2).

3.3. Elaboration of the switching table

Depending on the sector and the evolution of the flux and torque, the V_s and V_r voltage vectors can be used and selected, to comply with the flux and torque references. The commutation table for selecting the appropriate vectors is shown in Table 1, which is centered on the error of the fluxes, $\Delta\psi_s$ and $\Delta\psi_r$, the

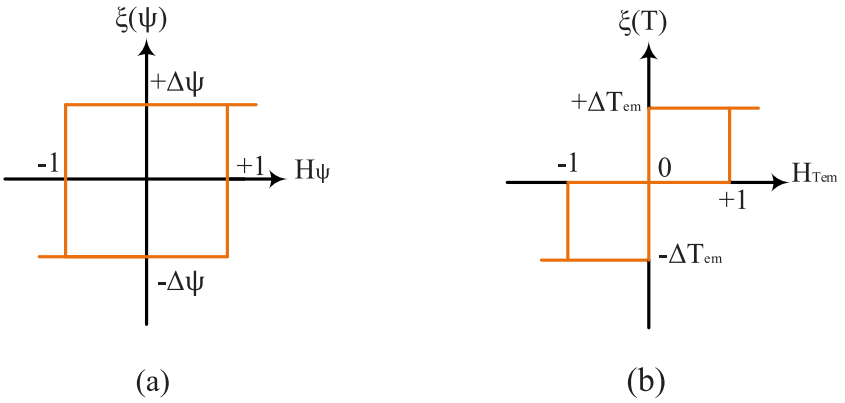

Fig. 2. Hysteresis controllers for (a) magnetic flux and (b) electromagnetic torque.

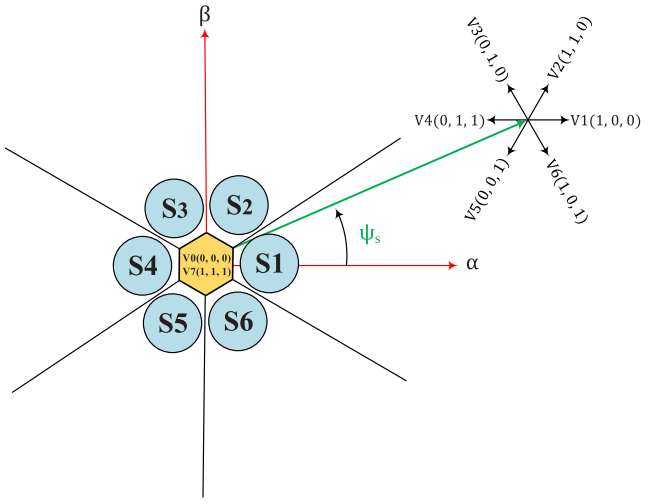

Fig. 3. Active voltage vectors and sectors of the flux vector space.

Table 1
The inverter sequences.

H_{ψ_s} or H_{ψ_r}	H_{tem}	Sector S_i					
		S_1	S_2	S_3	S_4	S_5	S_6
1	1	$v_2(110)$	$v_3(010)$	$v_4(011)$	$v_5(001)$	$v_6(101)$	$v_1(100)$
	0	$v_7(111)$	$v_0(000)$	$v_7(111)$	$v_0(000)$	$v_7(111)$	$v_0(000)$
	−1	$v_6(101)$	$v_1(100)$	$v_2(110)$	$v_3(010)$	$v_4(011)$	$v_5(001)$
0	1	$v_3(010)$	$v_4(011)$	$v_5(001)$	$v_6(101)$	$v_1(100)$	$v_2(110)$
	0	$v_0(000)$	$v_7(111)$	$v_0(000)$	$v_7(111)$	$v_0(000)$	$v_7(111)$
	−1	$v_5(001)$	$v_6(101)$	$v_1(100)$	$v_2(110)$	$v_3(010)$	$v_4(011)$

error of the torque ΔT_{em} and the location of the flux vectors ($i = 1, 2, 3, 4, 5, 6$), to control the flux and the electromagnetic torque of the DFIM, the operating principle of active voltage vectors and sectors of the fluxes vectors space is presented in Fig. 3 (Mahfoud et al., 2021b).

3.4. Syntheses of PI regulation speed

The proportional–integral (PI) controller is used for speed regulation in DTC. It is performed by comparing the speed reference signal to the actual measured speed value. Then the comparison error becomes the input of the PI controller.the transfer function TF dedicated from Eq.(5) of the speed as a function of torque is $\frac{1/f}{1+si/f}$. The pole placement method is used to determine the controller gains. Fig. 4 shows the speed PI controller diagram block.

from Fig. 5, the gain K is deduced by the projection of −45 on the phase diagram and the gain diagram to calculate the gains of the PI corrector by the expressions (17) and (18). $K_p = 0.776$ and $K_i = 28.74$ are the gains used in classic DTC.

$$CLTF\ (s) = \frac{1/f}{1 + si/f} = \frac{T}{G_0 * \tau}\left(1 + \frac{1}{T_i s}\right) = K_P + K_i \frac{1}{s} \tag{17}$$

$$\begin{cases} K_P = \frac{T}{G_0 * \tau} \\ K_I = \frac{K_P}{0.1 * J/f} \end{cases} \tag{18}$$

where: $T = J/f$ and $G_0 = 1/f$ and τ time constant.

Fig. 5 presents the Nyquist diagram of the response of the closed-loop system after correction. To study the stability of the system, the point (−1,0) is noticed that is to the left of the contour traced by the curve. so the system is stable.

Fig. 6 shows the response to a step, corrected by the closed-loop PI regulator of the speed transfer function without DTC. this response shows an acceptable overshoot and a rapid response time without static error.

4. Ant colony optimization algorithm:

4.1. Operating principle

The ACO technique is a metaheuristic inspired by the behavior of ants in their search for food. The ants begin to move randomly in their own environment. Then, once they have found food (ND), they return to their colony (NS) while leaving a trail of pheromone (Chiha et al., 2012). If other ants cross this path, they may be able to halt their random movements and join the marked path, reinforcing the optimum path on their return if it leads to food. At the same time, the shortest path will be more traveled, making it more fortified and appealing. The least fortified paths eventually disappear, forcing all ants to take the shortest path. Fig. 7 depicts the experience of choosing the shortest branch.

Each ant is considered an agent capable of generating solutions. The decision to take an ant to build a solution depends on two factors:

(a) Visibility factor: also called the gluttonous force noted η_{ij} where ij is the decision to be made. (b) Trace factor: τ_{ij} where ij is the decision to be made, the larger this value, the more interesting it has been in the past to make this decision.

Where the following relationship represents the probability that an item where a decision ij is chosen.

Each ant is regarded as an agent capable of generating solutions based on the decision to use an ant to construct a solution that is dependent on two factors:

(a) Factor of visibility: Also known as the gluttonous force noted η_{ij}, where ij is the decision to be made.

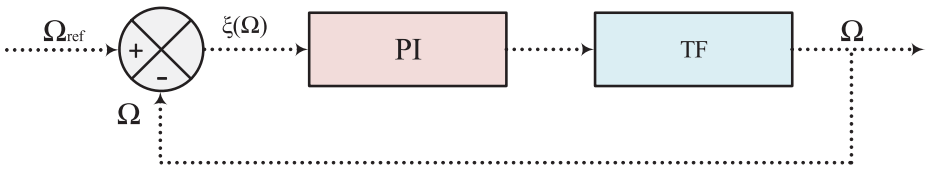

Fig. 4. Speed PI controller diagram block.

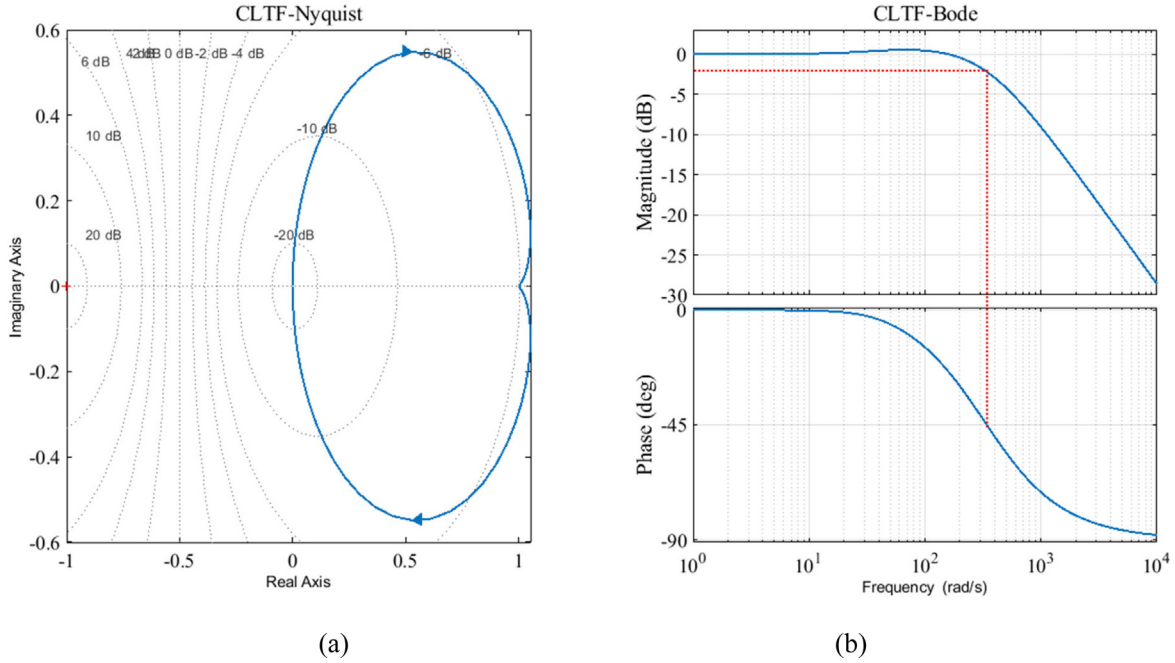

Fig. 5. Nyquist response (a) and bode diagram of CLFT.

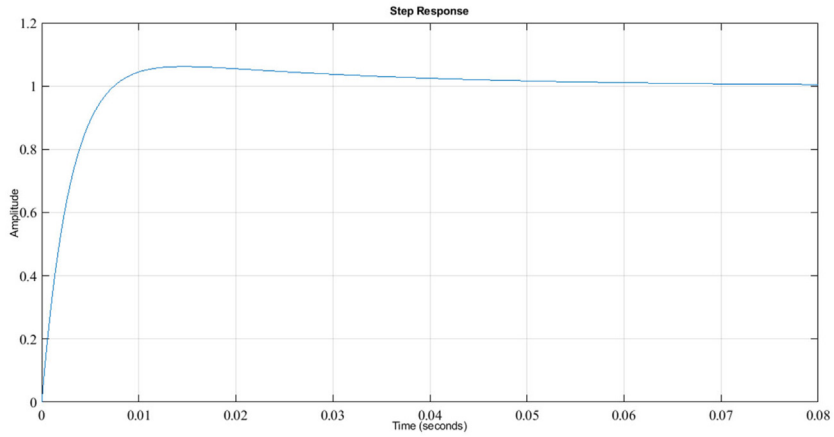

Fig. 6. Step response on the process after regulation.

(b) Trace factor: τ_{ij} where ij is the decision to be made, the higher this value, the more appealing, it has been to make this decision in the past.

Where the following relationship represents the likelihood that an element where a decision is made will be chosen.

$$P_{ij}^{k}\begin{cases}\dfrac{(\tau_{ij}(t))^{\alpha}(\eta_{ij}(t))^{\alpha}}{\sum_{ieN_i}(\tau_{ij}(t))^{\alpha}(\eta_{ij}(t))^{\alpha}}\\ 0\end{cases} \tag{19}$$

$\tau_{ij}(t)$: At time t trace amount of pheromones at (i, j) the corners

$\eta_{ij}(t)$: Visibility value between (i, j) corners. This value varies according to the criteria taken into consideration in solving the problem

α: Shows the relative importance of the pheromone trace in the problem

β: Shows the importance that given to visibility value

N_i: Set of the node points that have not been chosen yet

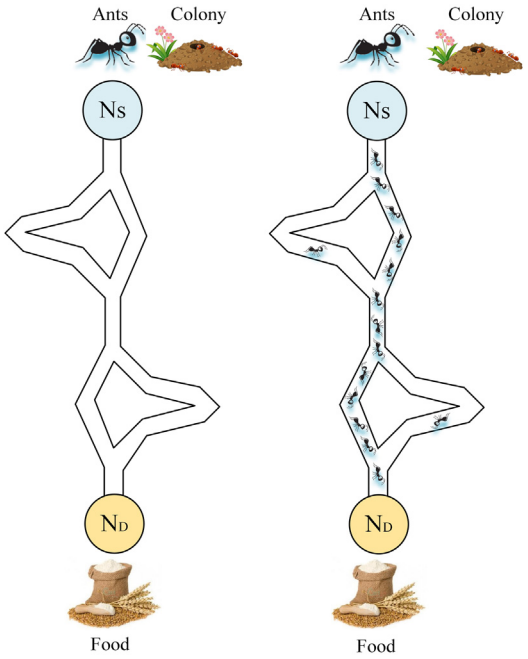

Fig. 7. Selection experiment of the shortest branches by a colony of ants.

4.2. PID controller design with ACO

Until now, some researchers have worked on PID optimization techniques with the ACO algorithm, employing a variety of approaches to improve the ACO's efficiency. Varol and Bingul (2004) used ACO to adjust the PID controller parameters for a second-order process with various cost functions. They discovered a significant improvement as compared to traditional adjusting techniques. Fig. 8 depicts the optimization of the PID controller using the ACO block structure.

To solve the problem of the design of the PID controller with the ACO algorithm, this may be described as a network problem, as shown in Fig. 9. Three different vectors were used to place all of the values for each parameter (K_P, K_I, K_D). To build a graphical representation of the situation, these vectors may be assumed to be roads between nests. During the tour, each ant must travel three nests by selecting the way between the beginning node and the end node. The ACO's objective is to identify the appropriate road with the lowest cost function (as stated in Eq. (25) between three nests. These ants lay down their pheromones at the beginning of every road. And after that, pheromones were updated towards updating pheromones in the reinforcement rule.

In this strategy, each ant updates the pheromones deposited on the track after performing a certain tour as the local pheromones update rules represented by the following expression follows Eq. (20).

$$\tau_{ij}(k) = \tau(k-1)_{ij} + \frac{0.01\theta}{J} \tag{20}$$

where
$\tau_{ij}(k)$ is pheromone value between nest (i) and (j) at the k. iteration.
θ is the general pheromone updating coefficient.
J is the cost function for the tour traveled by the ant.

In the global pheromone updating rule, pheromones of the paths belonging to the best tour Eq. (21) and worst tour Eq. (22) of the ant colony are updated as given in the follows:

$$\tau_{ij}(k)^{best} = \tau(k)_{ij}^{best} + \frac{\theta}{J_{bset}} \tag{21}$$

$$\tau_{ij}(k)^{worst} = \tau(k)_{ij}^{worst} - \frac{0.3\theta}{J_{worst}} \tag{22}$$

where τ^{bes} and τ^{worst} are the pheromones of the paths followed by the ant in the tour with the lowest cost value (J^{best}) and the highest cost value (J^{worst}) in one iteration, respectively. The pheromones of the paths belonging to the best tour of the colony are increased considerably, whereas those of the paths belonging to the worst tour of the iteration are decreased. After that, pheromone evaporation Eq. (23) allows the ant algorithm to forget its past history so that ACO can direct its search towards new directions without being trapped in some local minima.

$$\tau_{ij}(k) = \tau(k)_{ij_{ij}}^{\lambda} + \left(\tau(k)_{ij_{ij}}^{best} + \tau(k)_{ij_{ij}}^{worst}\right) \tag{23}$$

where λ is the evaporation constant (Varol and Bingul, 2004)

4.3. Fitness

The critical step in the execution of the ACO is to select the cost functions used to determine the suitability of each node. Some papers (Devasahayam and Veluchamy, 2017; Herlambang et al., 2019) use performance indices as cost functions. For this reason, in Herlambang et al. (2019), the authors compare separately and with a weighted combination three cost functions such as Integral Time Absolute Error (ITAE), Integral Absolute Error (IAE), and Integral Square Error (ISE). The latter has proven

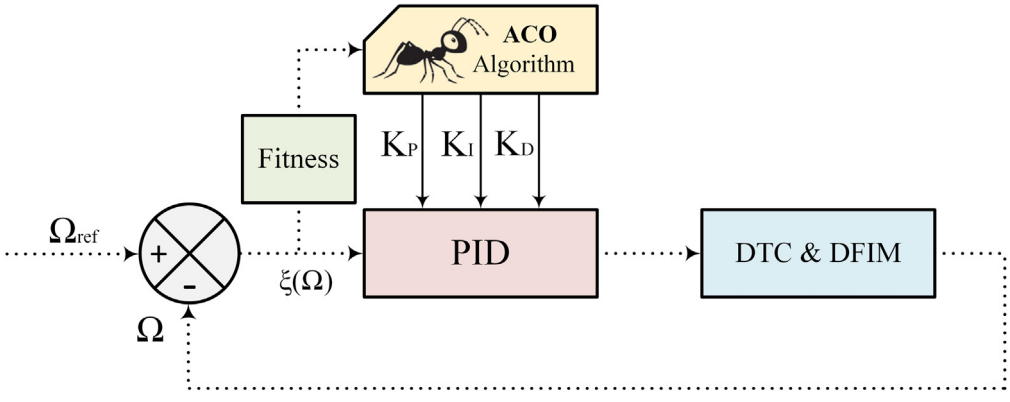

Fig. 8. Optimization of the PID Controller of ACO.

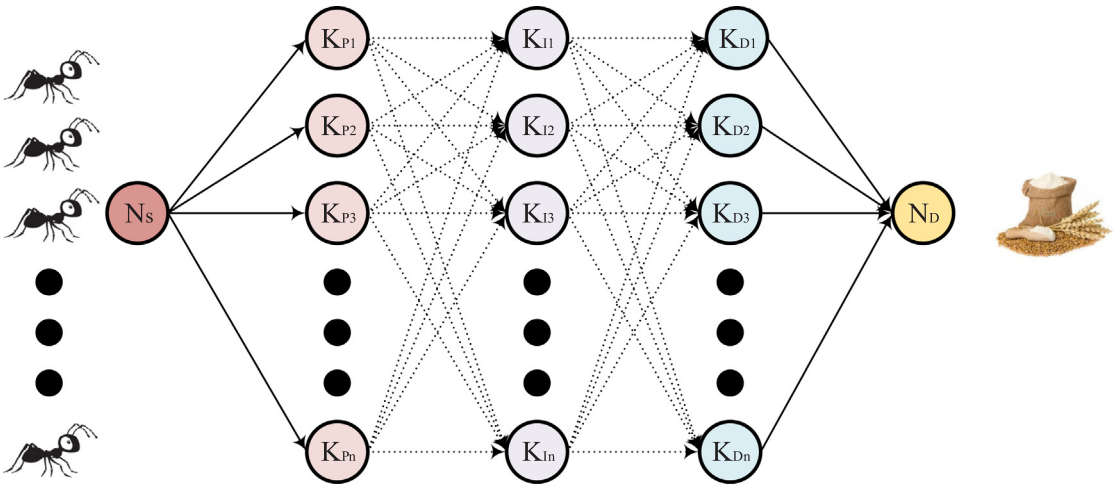

Fig. 9. Graphical representation of ACO for PID tuning process.

to be effective in terms of performance compared to other cost functions. For this reason, in this work, a weighted combination is used to increase the performance of the ACO, subsequently increasing the overall system, The performance indices should be described as follows (Kanojiya and Meshram, 2012):

$$ISE = \int_0^t e(t)^2\, dt \tag{24}$$

The PID controller is used to minimize the error signal e(t) which reduces the value of the specified performance indices, hence minimizing the equivalent value expressed by knots. With this minimization, knots will be formed. The node adequacy is defined by:

$$Fitness\ Value = \frac{1}{ISE} \tag{25}$$

4.4. ACO parameters

The steps of PID optimization with ACO are given in the algorithm of ACO presented below and the flowchart of the ACO steps is illustrated in Fig. 10. In this section, PID controller parameters were coded by 5000 nodes. In other words, one node represents a solution value of the parameters (K_P, K_I and K_D) Thus, the bigger the number of used nodes, the more accuracy trails are updated. Optimal ACO parameters ($\theta = 0.06$, $\lambda = 0.95$) were obtained at the end of numerous experiments.

The choice of the parameters of the ACO algorithm is an essential step to convergence towards the optimal values in a reduced time. In this article, the approach is proposed to validate two criteria (optimal values and reduced time).

The parameters of the Ant Colony Optimization algorithm (Var_{Pmax}, Var_{Pmin}, Var_{Imax}, Var_{Imin}, Var_{Dmax}, Var_{Dmin}, and n_iter) must be initialized to very large values ($Var_{Pmax} = Var_{Imax} = Var_{Dmax} = 100$, $Var_{Pmin} = Var_{Imin} = Var_{Dmin} = -100$, n_iter $= 100$) to increase the probability of getting the best values for K_P, K_I, and K_D, but in this case, the system only converges after a certain time, after this step the algorithm parameters must be reduced closest to the optimum gains found previously, which reduces the iteration number minimizing the execution time, Table A.1 in the Appendix shown the ACO parameters.

Algorithm: Ant Colony Optimization Algorithm

Begin
Step 1. Initialize the algorithm parameters (n_iter, NA, α, β, Eva, n_para, n_node, LB, LU).
Create a pheromone matrix and use a uniform distribution to generate random potential solutions for the parameters (K_P, K_I and K_D).
Step 2. Run the DTC control and calculate the fitness of the weighted cost functions.
Step 3. Choose the successive node with probability using Eq. (19).
Step 4. Display the optimum values of the optimization parameters (K_P, K_I and K_D).
Iterate from step 2 until the maximum of ants is reached.
Step 5. Use pheromone evaporation given by this Eq. (21), to reinforce the best tour and allow the forgetfulness of bad choices using Eq. (22):
Step 6. Globally update the pheromone using Eq. (23), according to the optimum solutions calculated at Step 5.
Iterate from step 2 until the maximum of iterations is reached.
Step 7. Choose the path with the maximum pheromone.
End

5. Simulation procedure and interpretation:

The proposed strategy of the DTC control using a PID controller based on ACO of a DFIM using ISE is shown in Fig. 11.

The global system is realized on the Matlab/Simulink platform to validate the theoretically proposed approach. The values of the PID controller parameters optimized by the ACO are within the variation bands shown in Table 2. The global system is configured with the parameters in Table A.1 and subjected to speed and torque references. The simulation results for the two strategies (conventional DTC and ACO-DTC) were tested using a machine along with the following steps:

1. A reference speed step of 78.5 rad/s is applied at no load from $t = 0.6$ s to $t = 1.05$ s.
2. An instantaneous change in speed is increased at 157 rad/s from $t = 1.05$ s to $t = 2.05$ s, and from $t = 1.1$ s to $t = 1.6$ s a load torque of 10 N m is applied to the machine.

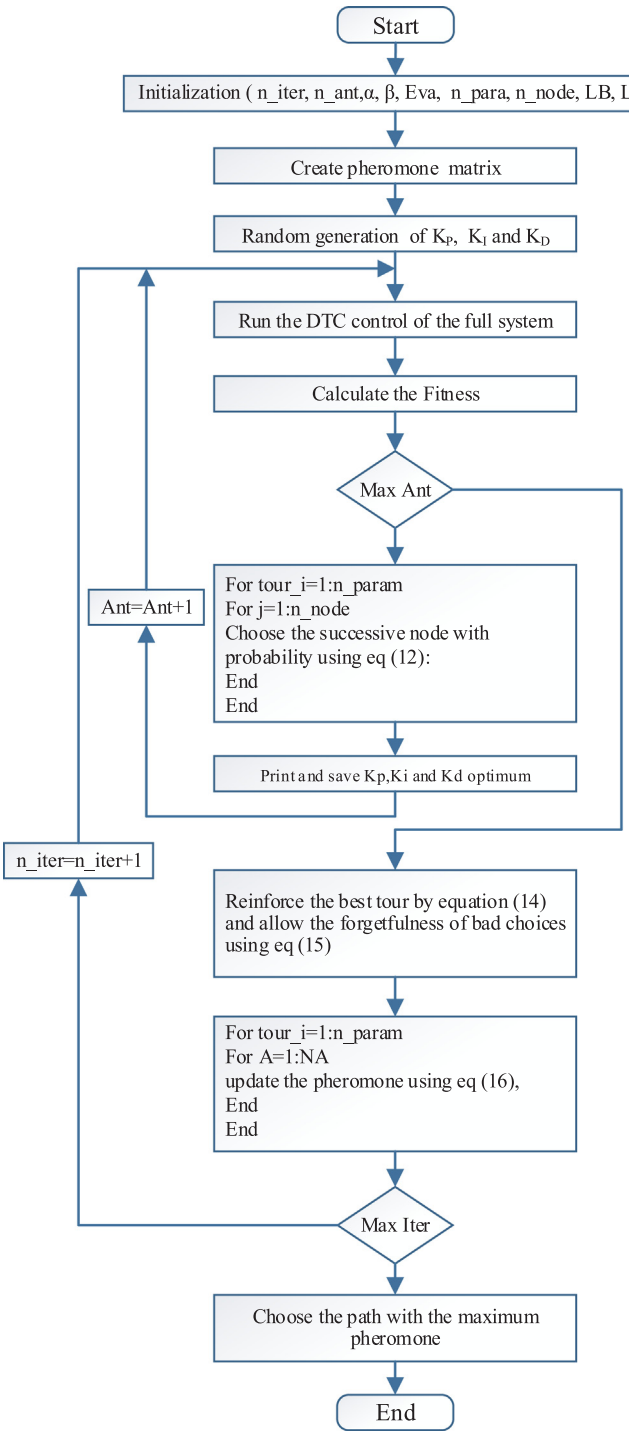

Fig. 10. ACO flowchart for Optimization of the PID Controller.

3. from $t = 2.05$ s to $t = 2.3$ s and from $t = 2.6$ s to $t = 3$ s a progressive minimization of the speed in the form of an affine function to test the tracking of the reference speed.
4. from $t = 2.3$ s to $t = 2.6$ s the machine is stopped to reverse the direction of rotation.
5. from $t = 3.05$ s to $t = 4.05$ s the direction of the speed is reversed by a value of -157 rad/s and the application of torque of -10 N m to test the behavior of the control in the opposite direction.

Table 2
The PID parameters band.

PID parameters	K_P	K_I	K_D
Maximum value	100	5	1
Minimum value	0	0	0

Table 3
Optimal gains generated by ACO.

Controller parameters	ACO-DTC
K_P	46.5947
K_I	3.54094
K_D	0.076549

6. from $t = 4.05$ s to $t = 5$ s an instantaneous reduction in speed to -78.5 rad/s without load.

All the parameters of the system are initially configured by:

- The sampling frequency is: $f_s = 10$ kHz.
- The widths of the hysteresis bands are: $\Delta T_{em} = \pm 0.01$ N m, $\Delta \Psi_s = \pm 0.001$ N m and $\Delta \Psi_r = \pm 0.001$ N m.

The proposed intelligent ACO-DTC strategy is examined in various operating situations using Matlab/Simulink. Tables A.1 and A.2 in the appendix show the critical parameters of the ACO algorithm and DFIM, while Table A.3 presents the abbreviations of the words used in this article. The optimal values considered for the PID regulator parameters without optimization and optimized by ACO with an ISE cost function are shown in Table 3.

The DFIM's performance is shown in figures from 12 to 22. When the motor operates at a speed of 78,5 rad/s, then increases instantly to 157 rad/s, then decreases along a linear slop to -157 rad/s, then increases instantly to -78 rad/s, the motor is subjected to 10 N m and -10 N m applied at time t = 0.75 s and time t = 2.75 s.

- Fig. 12(a, b, c) shows the motor's responses in speed, which is controlled smoothly even with a small load variation. When the motor runs at speeds of 78,5 rad/s and 157 rad/s with an initial load of 0 N m until 0.6 s and is increased to 10 N m after 0.6 s, the speed responses demonstrates the speed characteristic motor's improved by the intelligent ACO-DTC technique, one will find the annulation of the overshoot, as well as the reduction of response time, rejection time, and undershoot with rates of 49.5%, 82.8%, 100%, and 19.92% respectively in comparison to the classical DTC.
- Fig. 13 depicts the torque responses of the motor under various control strategies. Based on this statistic, we can see that the torque response of the ACO-DTC intelligent approach has less ripples than the classic DTC, resulting in an improvement rate of 21.88%. For ACO-DTC/DTC, the torque is controlled smoothly, and there is less overshoot during a sudden load from 1.1 s and 3.1 s for different strategies.
- Figs. 14, 15, 16, and 17 depict the characteristics of stator and rotor currents, as well as their THDs. Based on these figures, we can see that the stator and rotor current are sinusoidal and shapes deviate from their ideal forms, as expressed by THDs of 12 % and 7.85 %, respectively, resulting in medium THDs causing torque ripples of 2445 N m for the conventional DTC.
- Figs. 18, 19, 20, and 21 depict the waveforms of stator and rotor currents of the ACO-DTC, as well as their THDs. from these figures, we can notice that the stator and rotor current are sinusoidal and close to their forms, as expressed by THDs

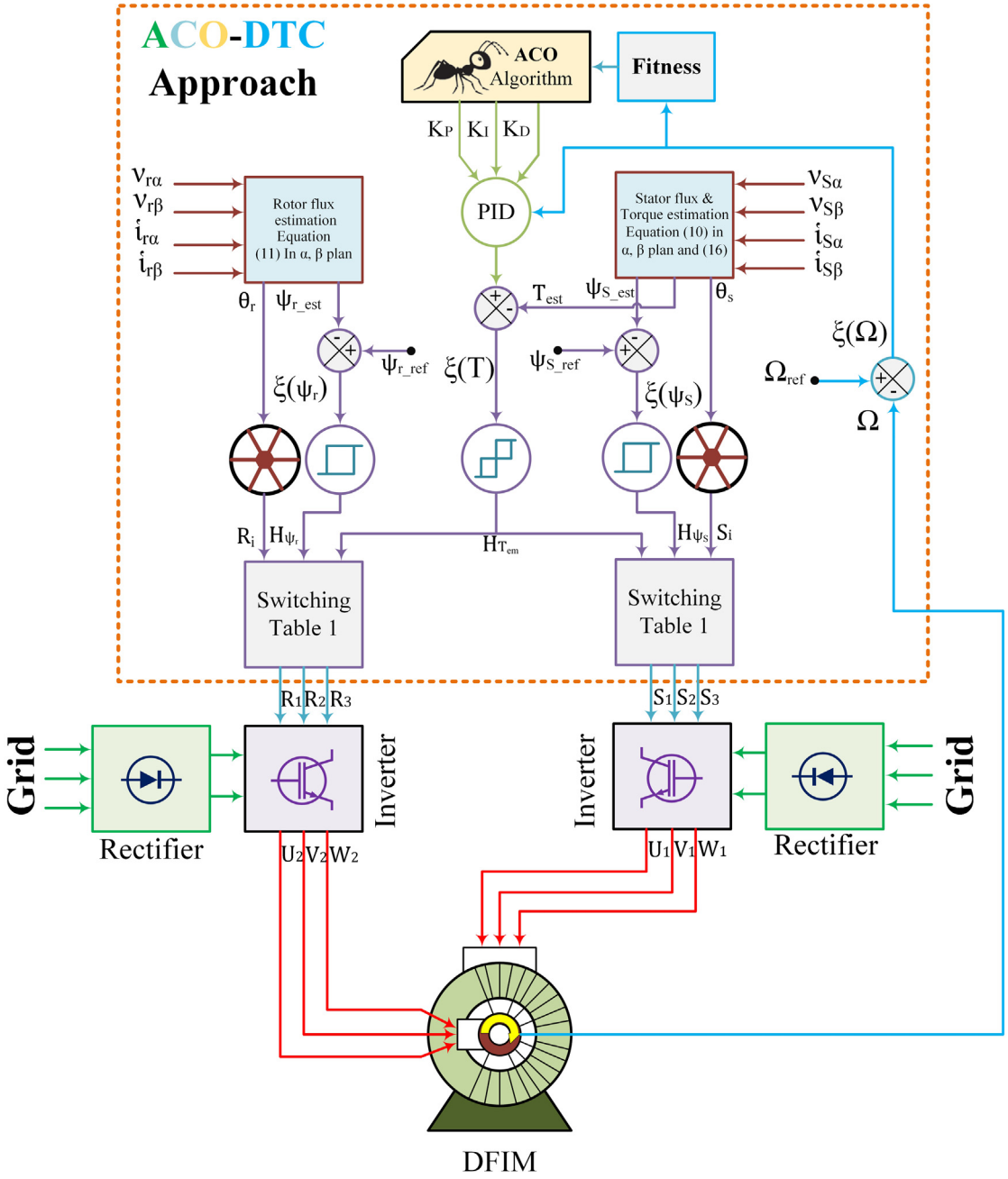

Fig. 11. Smart ACO-DTC control structure of the DFIM.

of 7.19% and 4.89%, respectively, arriving at enhancement of 40.08% and 37.71% respectively, resulting in good THDs causing torque ripples of 1.91 N m.

- Fig. 22 illustrates the stator and rotor fluxes characteristics of traditional DTC and ACO-DTC, which improve fluxes amplitudes by 26.66% and 19.45%, respectively.

In comparison of ACO-DTC to a traditional DTC, the DFIM quickly achieves its value as a reference torque. Furthermore, the torque is well controlled in fluctuating load situations. As shown in Fig. 12, the proposed DTC based on ACO has a good response in terms of speed, reaching the desired speed very quickly with little response time and without overshoot. Furthermore, the speed can be controlled smoothly in the event of a sudden change in loads, the load moves from 0 N m to 10 N m in 1.05 s and from 0 to −10 N m in 3.1 s. Finally, based on the overall analysis, the proposed strategy outperforms the conventional DTC. The proposed strategy can be used to control the motor with minimal torque ripples.

Based on the previous interpretations and the various performances presented in Table 4, our ACO-DTC proposed in this article has confirmed the target set in the introduction, demonstrating the robustness of this technique in terms of speed, fluxes, and torque ripples, and THDs of currents.

The enhancements made by ACO-DTC to the traditional DTC control, enable the DFIM to be controlled more reliably under a variety of operating situations. The reason for this is that the ANN-DTC strategy adapts to the machine's parametric variation, making it the best choice for a speed drive.

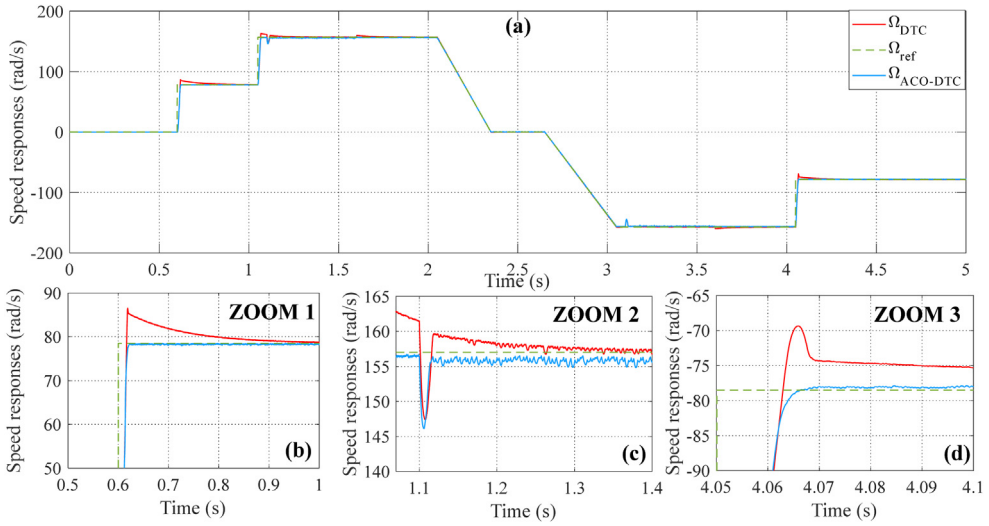

Fig. 12. Speed responses (a, b, c, d) of both strategies.

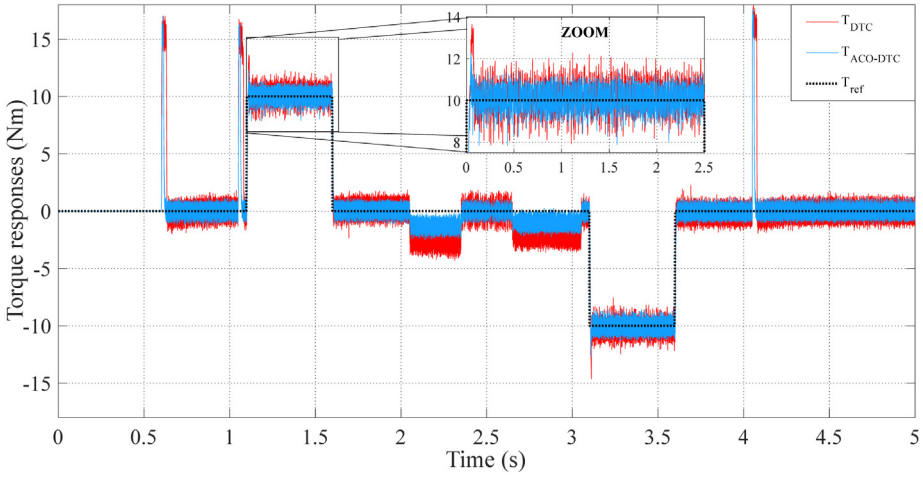

Fig. 13. Torque responses of the DTC and ACO-DTC.

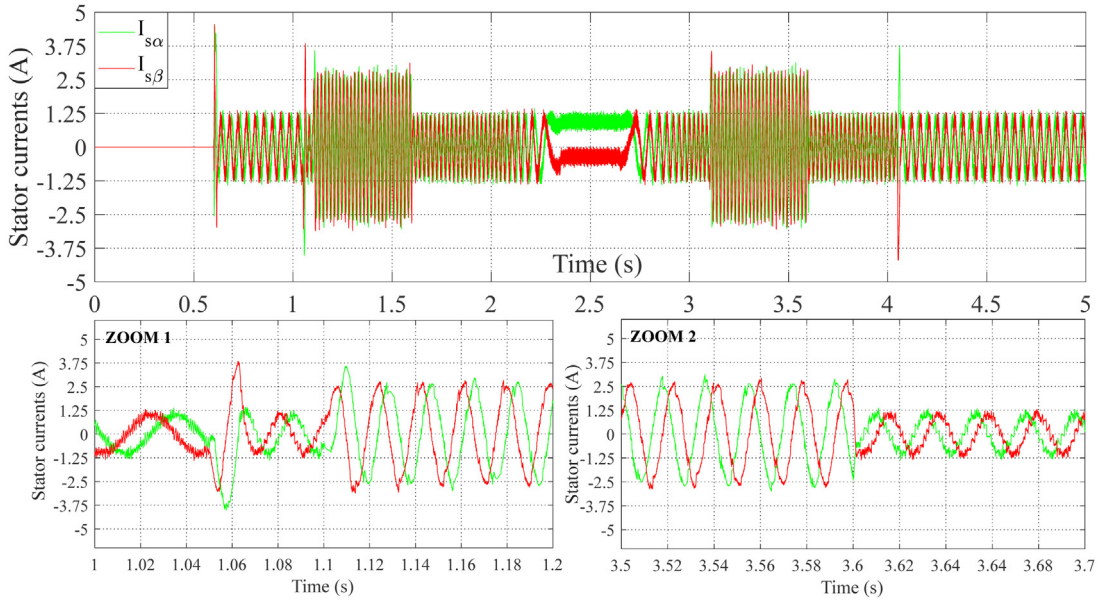

Fig. 14. Stator currents of the DTC.

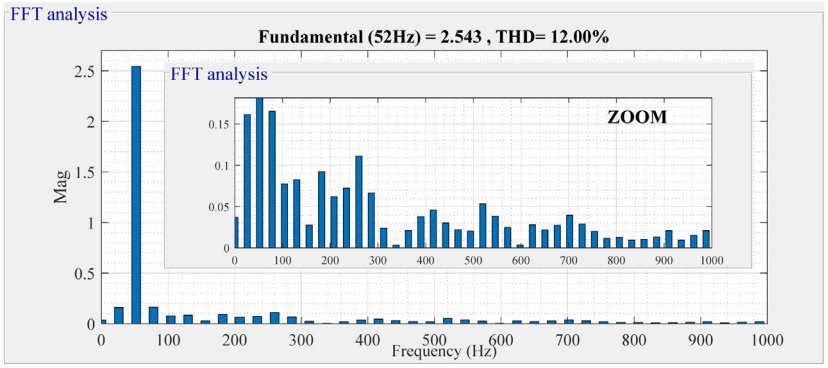

Fig. 15. Stator current THD of the DTC.

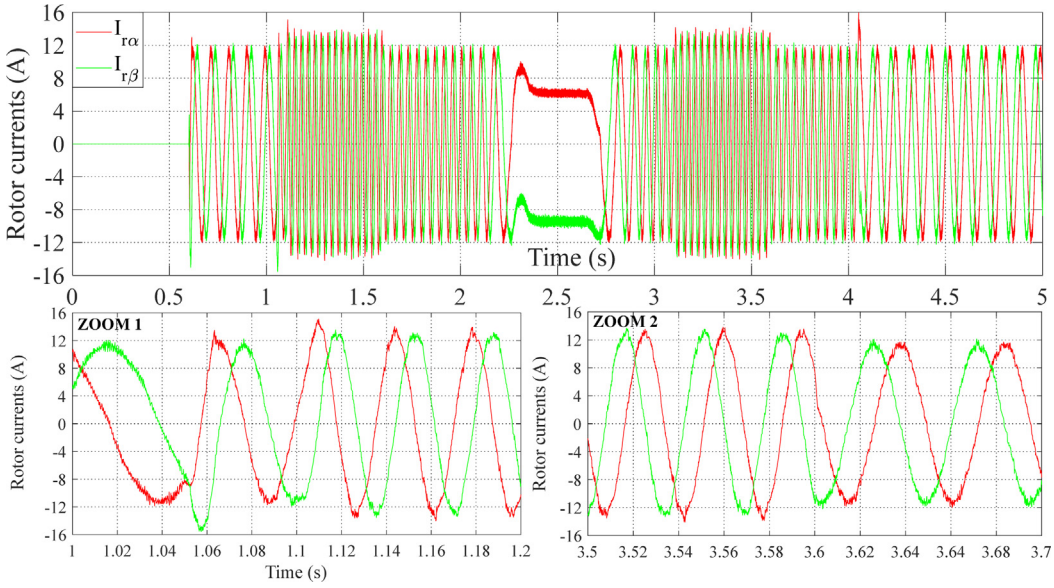

Fig. 16. Rotor currents of the DTC.

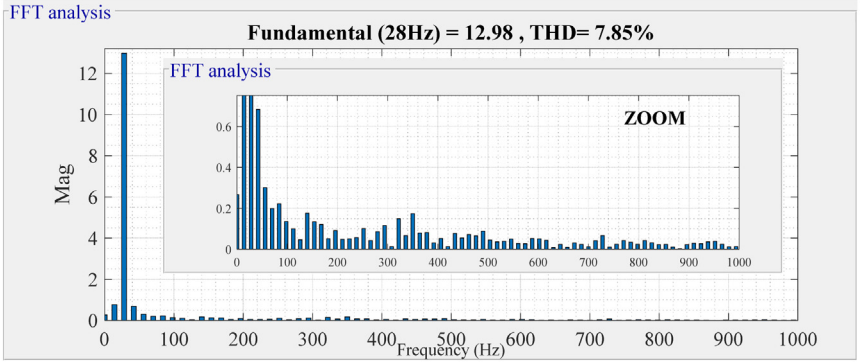

Fig. 17. Rotor current THD of the DTC.

6. Discussion and comparison

In the technical literature, there are several approaches used with the DFIM to control the motor at various speeds and torques. One of these is the FOC control established by Abderazak and Farid (2016), which is very sensitive to the parametric variation of the motor due to its mathematical expressions rich in machine parameters, making it less robust. This strategy has a response time of 0.56 s and torque ripples of 2.5 N m. In Hasse (1968), the authors used the sliding mode control, which is known as the chattering phenomenon, which reduces the robustness of this approach in terms of performance. This strategy has a response time of 0.19 s and torque ripples of 2.5 N m. Because of the disadvantages of the controls mentioned above, the DTC becomes the most appropriate solution, and among the methods used to increase its robustness are artificial intelligence techniques. The authors of El Ouanjli et al. (2018) replaced the hysteresis comparators and switching tables with fuzzy logic controllers, that minimize torque ripples up to 1.14 N m and response time to 0.28 s, while the authors of Mahfoud et al. (2021a) optimized the

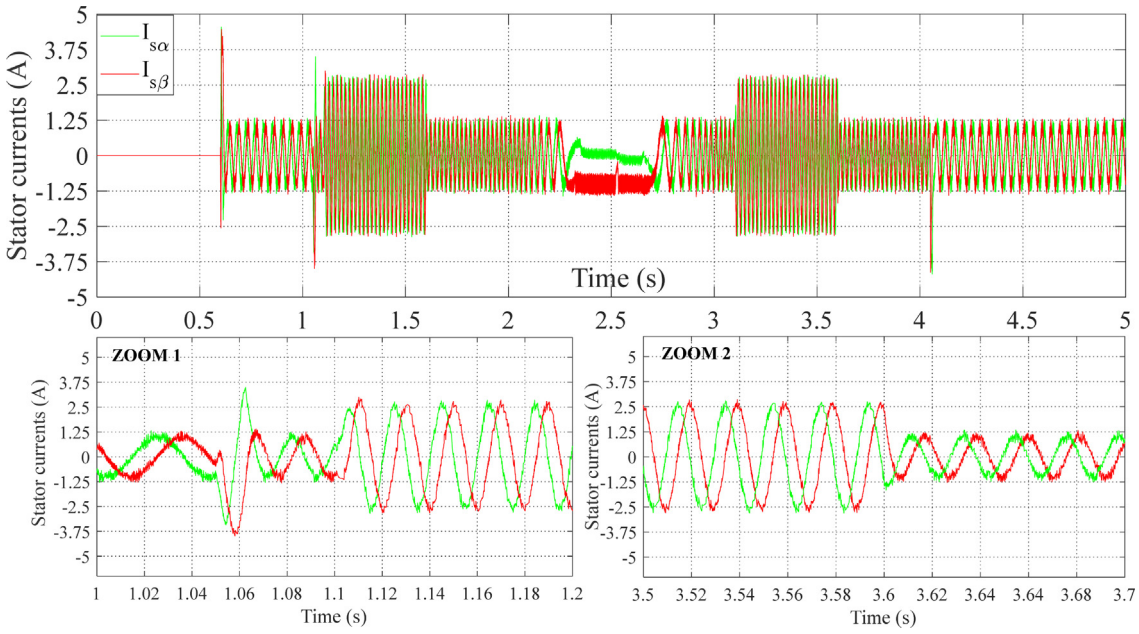

Fig. 18. Stator currents of the ACO-DTC.

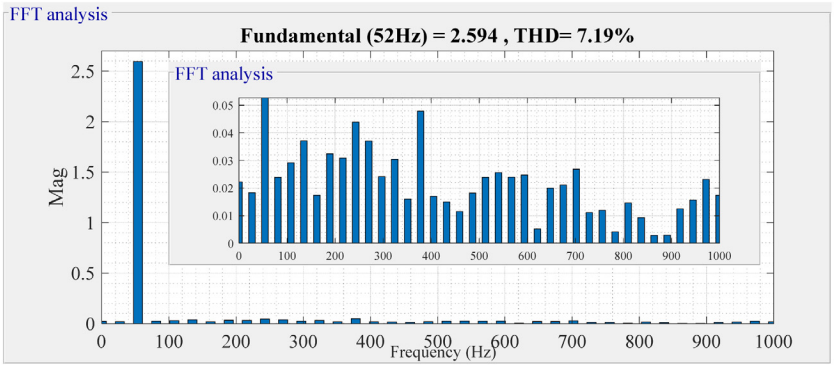

Fig. 19. Stator current THD of the ACO-DTC.

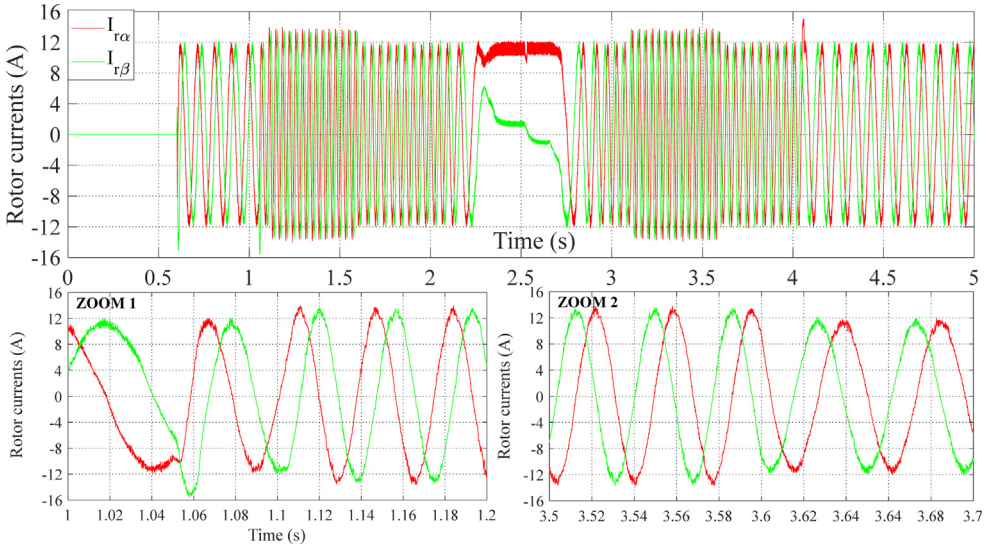

Fig. 20. Rotor currents of the ACO-DTC.

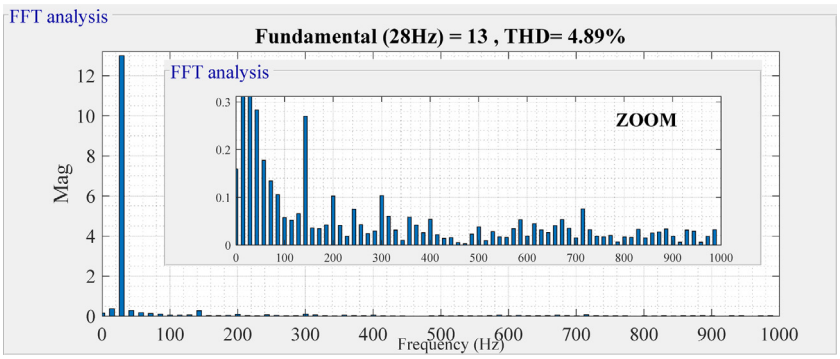

Fig. 21. Rotor current THD of the ACO-DTC.

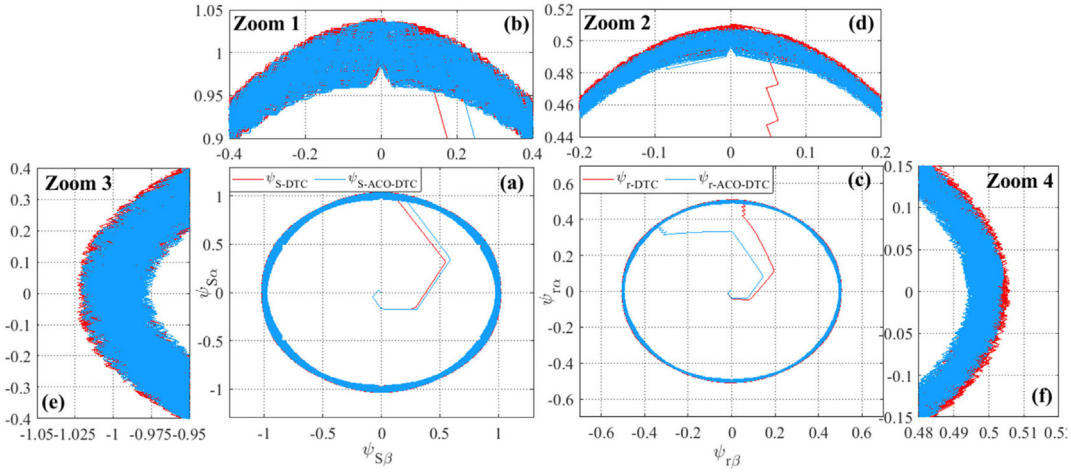

Fig. 22. Stator and rotor fluxes of both strategies.

Table 4
Performance measures DTC classic and ACO-DTC.

Performances	Characteristics	DTC	ACO-DTC	Improvements (%)
Ω	Response time (ms)	86	16.5	80.81
	Overshoot (rad/s)	8.02	0	100
	Rejection time (ms)	183.45	14.73	92
	Undershoot (rad/s)	13.91	10.26	26.24
T	Ripples (N m)	2.445	1.91	21.88
ψ_s	Ripples (wb)	0.06135	0.04311	29.73
ψ_r	Ripples (wb)	0.0131	0.00971	25.88
i_{sa}	THD (%)	12	7.19	40.08
i_{ra}	THD (%)	7.85	4.89	37.71

gains of the DTC control algorithm to have a good DFIM behavior in front of motor parameter variation. In the case of the GA-DTC approach or optimization algorithms. The ACO-DTC strategy we propose allows us to get the best performance possible, as seen in the following table. The next table illustrates the performance of several strategies applied to the DFIM.

The histograms in Figs. 23 and 24 describe the speed response time and the amplitudes of the torque ripples established by each control. From Fig. 23, we can say that the fastest control is the one with the smallest response time, which is presented by the proposed control ACO-DTC, and according to the histogram in Fig. 24, the control that presents fewer ripples is the FL-DTC one. This is normal because this control allows replacing the hysteresis comparators with fuzzy controllers, it is well known that the main cause of important ripples in the torque is the frequent switching of the hysteresis comparators.

Table 5
Comparison between our proposal and some controls strategy published recently.

Publication reference	Approaches	Response time (s)	Torque ripples (N m)	Robustness
Amezquita-Brooks et al. (2015)	Field oriented control	0.56	2.5	Not robust
Abderazak and Farid (2016)	Sliding mode control	0.19	2.4	Not robust
Classical DTC studied in this work	Classical DTC	0.0507	2.445	Robust
El Ouanjli et al. (2018)	FL-DTC	0.28	1.14	Robust
Mahfoud et al. (2021a)	GA-DTC	0.018	2.05	Robust
Proposal technique	ACO-DTC	0.0165	1.91	Robust

7. Experimental validation and interpretation

7.1. Presentation of the experimental banc

A practical solution is being implemented to validate the performance of the ACO-DTC nonlinear control. The control system is based on the DS1104 R&D Board Controller developed by dSPACE. Communication between the Simulink model and the DS1104 Board is provided by the Real-Time Interface (RTI) library. This structure is housed in an electronic device that facilitates the transfer of information between the software and the physical part of the system. The hardware component of the control board is responsible for application administration as well as the generation of PWM control signals in 0/5 V TTL logic. The inverters

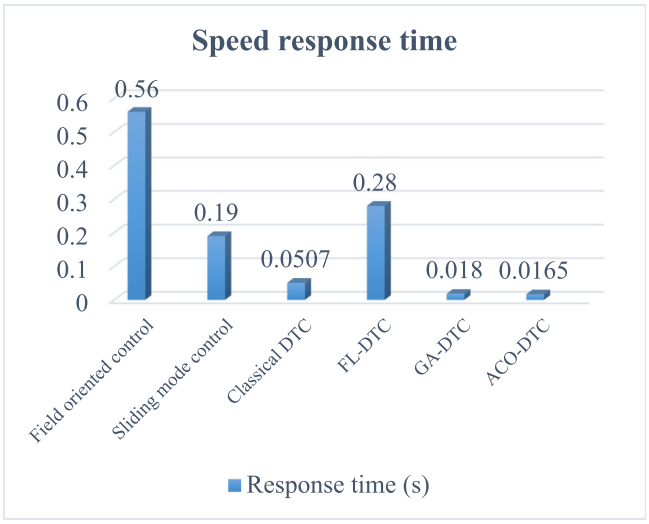

Fig. 23. Different speeds response time of various techniques for DFIM.

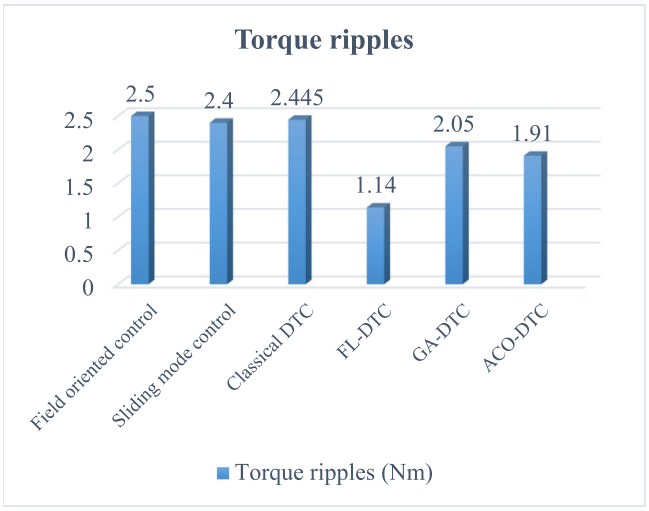

Fig. 24. Different torque ripples of various techniques for DFIM.

require TTL/CMOS 0/15 V matching driver boards to drive the IGBTs using the TMS320F240 slave DSP. The software section consists of a modeling tool (Matlab/Simulink) that allows users to program the application in question in real-time using blocks that have been specifically stored in the Toolbox Real-Time Interface (RTI) library. In addition, the RTI has the ability to graphically configure inputs and outputs.

In addition, the second piece of software called "ControlDesk" is responsible for loading the source code that is compiled and transformed into C on the DS1104 R&D board using the Real-Time Workbench (RTW) tool. As shown in Fig. 26, the second use of ControlDesk is the development of user interfaces for real-time control and the saving of programs in Matlab/Simulink-compatible files, as well as the monitoring of the evolution of the

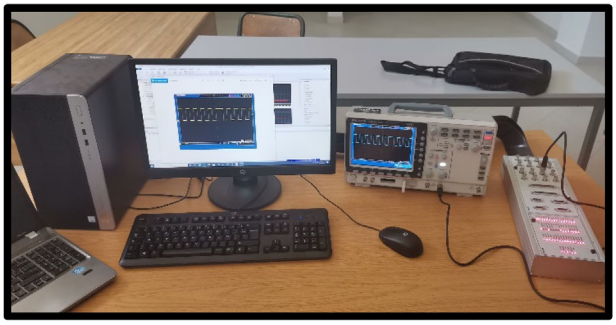

Fig. 25. Configuration diagram of the dSPACE controller board with DFIM.

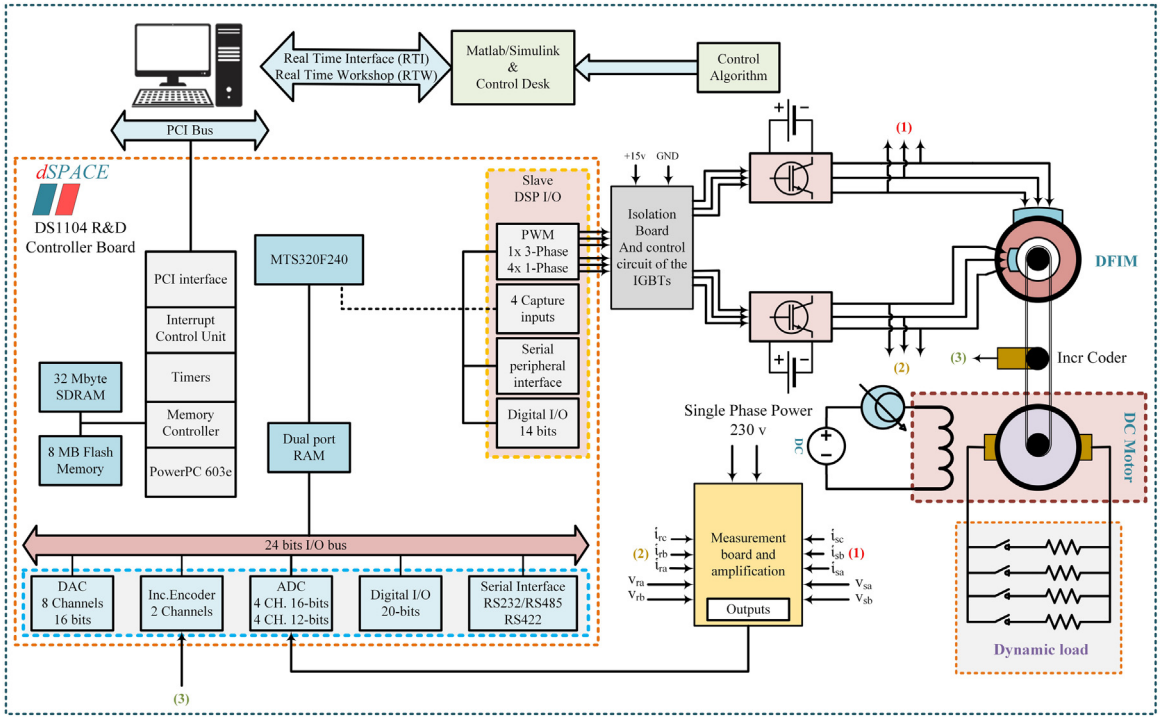

Fig. 26. Configuration diagram of the dSPACE controller board with DFIM.

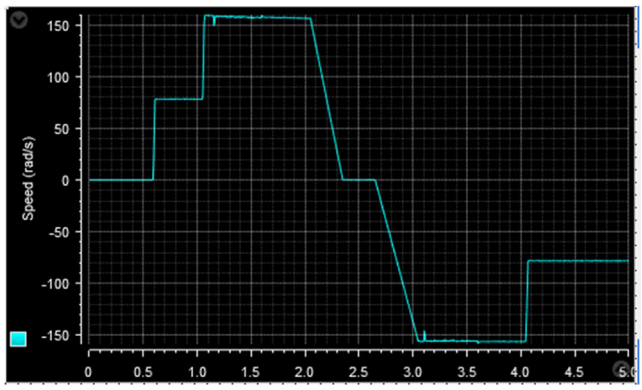

Fig. 27. Speed of the ACO-DTC.

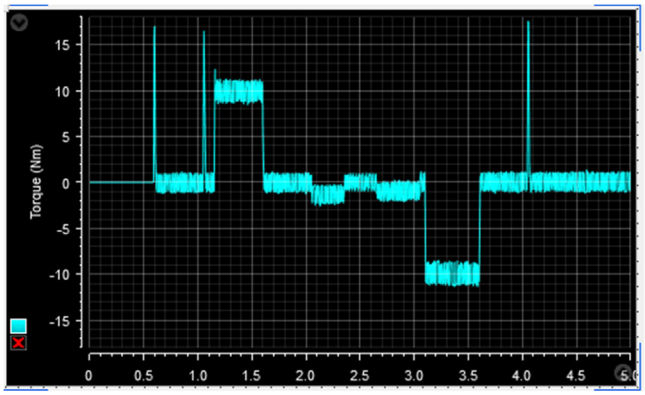

Fig. 28. Torque of the ACO-DTC.

measured and calculated data in real-time. The following are the main steps in prototyping graphics user interfaces:

1. Using the Simulink modeling tool to build the control system.
2. Simulating the system to generate the various control results.
3. Using the Real-Time Workshop, a C-language application is downloaded into the dSPACE environment (RTW).
4. Real-time execution of the global model using the R&D DS1104 Board. The R&D DS1104 controller is equipped with the main processor (MPC8240) with a clock rate of 250 MHz. Figs. 25 and 26 show the experimental banc and the diagram of the connection between the dSPACE Board and the DFIM, respectively. The dSPACE board and the Real-Time Workshop tool were used to carry out experiments as part of the experimental validation of the proposed ACO-DTC intelligent control.

7.2. Results interpretation

Following a variable speed setpoint in both directions is applied on the proposed ACO-DTC and DFIM control, either at no load or at load with values of 10 N m and −10 N m, to test the behavior of the system in these different working conditions, validating the objectives previously planned through experimentation on dSPACE DS1104.

From Figs. 27, 28, 29, 30, and 31, it can be seen that the results are similar to the simulation results. During an abrupt change in speed from 78.5 to 157 and from −157 to −78.5, the transition is made quickly without any overshoot in the forward and reverse directions. The abrupt changes in reference values induce peaks in the speed curves and the stator and rotor phase currents have a sinusoidal shape that varies according to the load, at the times

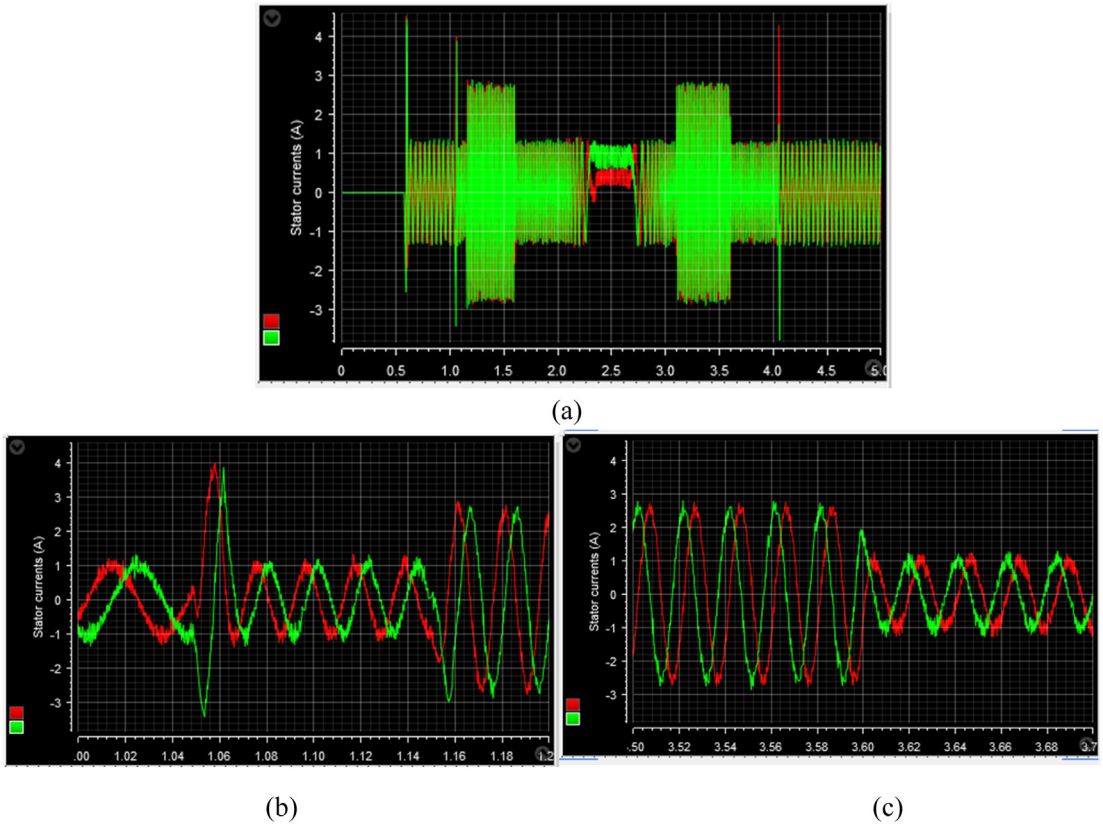

Fig. 29. Stator currents of the ACO-DTC, (b) and (c) zooms of currents from 1 s at 1.2 s and from 3.5 s at 3.7 s respectively.

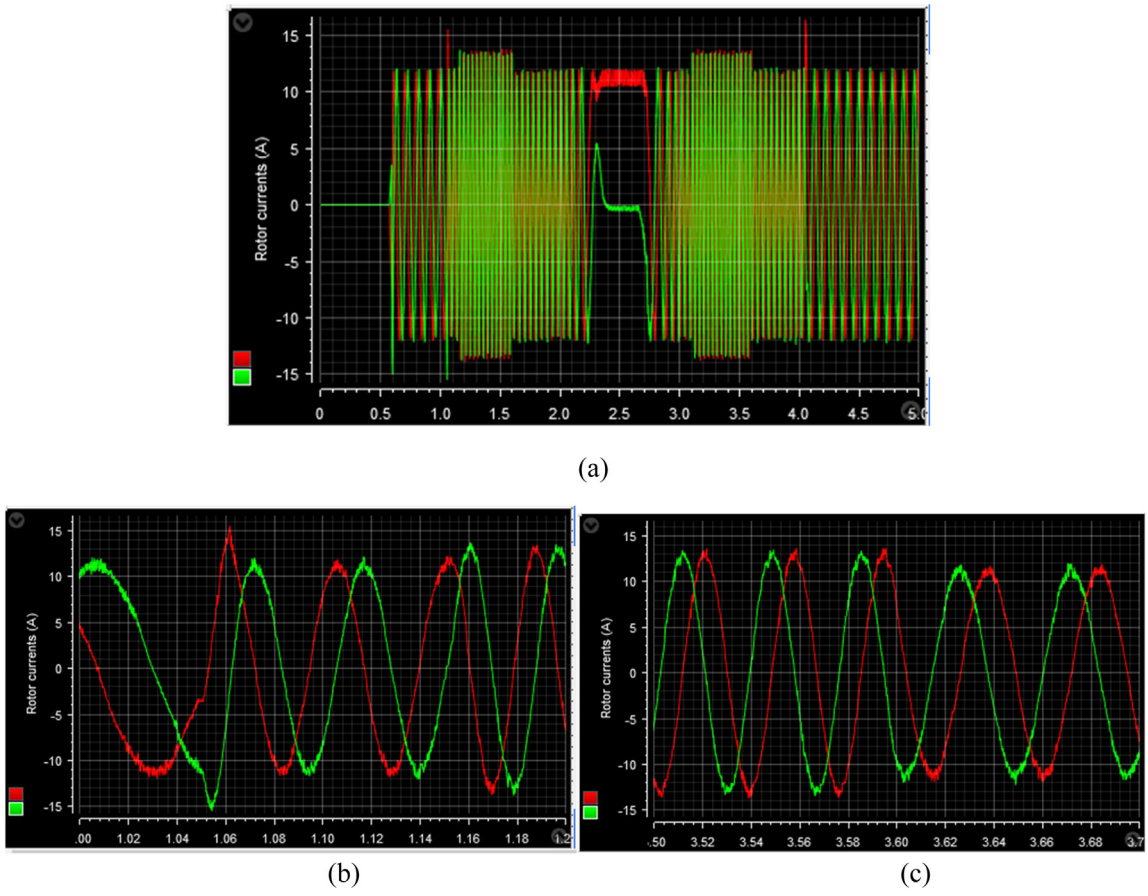

Fig. 30. Stator currents of the ACO-DTC, (a) and (b) zooms of currents from 1 s at 1.2 s and from 3.5 s at 3.7 s respectively.

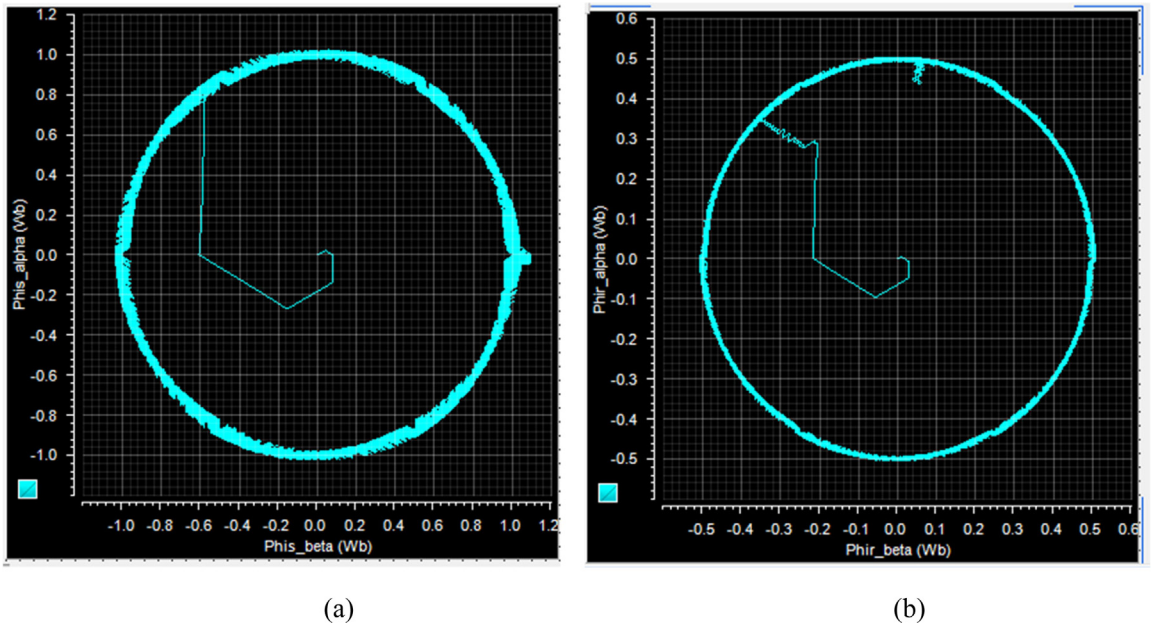

Fig. 31. Stator (a) and rotor (b) fluxes of the ACO-DTC.

of torque applications with a high correspondence between the simulation results and the field results (Figs. 29 and 30)

Fig. 27 shows steps of several speed levels [78.5 157 −78.5 157][rad/s]. The speed response is very fast (simulation and practice).it is also noticeable that the speed is established at the set values with good dynamics and negligible overshoots and without static errors, noting that there is a slight increase in torque ripples in practice related to measurement noise and parameterization of the control and the machine as shown in Fig. 28.

Table A.1
Parameters of the ACO Algorithm and DFIM.

Symbols	Value
n_eter	300
n_ANT	30
α	0.8
β	0.2
Eva	0.9
n_par	3
n_node	5000
Pn	1.5 Kw
Vs	400 v
Vr	130 v
P	2
F	50 Hz
Rs	1.75 Ω
Rr	1.68 Ω
Ls	0.925 H
Lr	0.104 H
M	0.165 H
f	0.0027 kg m^2/s
j	0.01 kg m^2

Table A.2
Nomenclature.

Parameters	Description
$v_{s\alpha}$, $v_{s\beta}$, $v_{r\alpha}$, and $v_{r\beta}$	Stator and rotor voltages in (α, β) plan
U_{dcs} and U_{dcr}	Stator and rotor direct voltages
$i_{s\alpha}$, $i_{s\beta}$, $i_{r\alpha}$, and $i_{r\beta}$	Stator and rotor currents in (α, β) plan
$\psi_{s\alpha}$, $\psi_{s\beta}$, $\psi_{r\alpha}$, and $\psi_{r\beta}$	Stator and rotor fluxes in (α, β) plan
R_s, R_r	Stator and rotor resistors
L_s, L_r	Stator and rotor inductors
L_m	Mutual Inductance
p	Number of pairs of poles
ω_r	Rotor angular speed
ω_s	Stator angular speed
Ω	Rotation speed
T_{em}	Electromagnetic torque
T_r	Resistant torque
f	Viscous friction coefficient
J	Moment of inertia
n_eter	Iteration number
n_ant	Ants number
Eva	Evaporation rate
n_node	Nodes number
n_par	Parameters number

Table A.3
Abbreviation table.

Abbreviation	Wording
DFIM	Doubly Fed Induction Motor
IM	Induction Motor
DTC	Direct Torque Control
FOC	Field Oriented Control
DFOC	Direct Field Oriented Control
IFOC	Indirect Field Oriented Control
PWM	Pulse Widht Modulation
GA	Genetic Algorithm
GA-DTC	Genetic Algorithm-Direct Torque Control
ACO	Ant Colony Optimization
GWO	Grey wolf optimization
PSO	Particle swarm optimization
EP	Evolutionary Programming
ACO-DTC	Ant Colony Optimization-Direct Torque Control
ANN-DTC	Artificial Neuron Network-Direct Torque Control
PID	Proportional Integrator Derivator
FOPID	Fractional Order Proportional Integrator Derivator
ZN	Ziegler Nicholas
DTFC	Direct Torque Fuzzy Control
DTNC	Direct Torque Neural Control
DTNFC	Direct Neural Fuzzy Torque Control
ANFIS	Adaptive Neuro-Fuzzy Inference System

Fig. 31 shows the circular curves of the stator and rotor fluxes which show the keeping of the fluxes within the band of the hysteresis comparators, the results obtained are similar to the simulation results.

According to the simulation results on Matlab/Simulink and the experimental results extracted from the Controldesk, the proposed ACO-DTC control has shown great flexibility and adaptability with such a change of speed or torque, deducing that this strategy can be the right choice for the implementation within the variable speed drives designed to control the DFIM.

Conclusion: In this study, a new proposed approach based on PID is optimized by using an optimization algorithm, known in terms of ACO for DTC applied in DFIM. This structure is simulated on Matlab/Simulink and validated experimentally on the Dspace DS1104 board. This work presents an improvement to the behavior of the classical DTC by optimizing and generating in each period the PID parameters KP, KI, and KD, to adapt the system to its non-linearity. The ACO-DTC control proved many improvements in performance, such as speed overshoot and rejection time, fluxes and torque ripples, and currents THD. The enhancements that are being made to the DFIM performances are summarized by the following points:

- removing speed overshoot in all reference speed variations with and without torque
- reducing the rejection time with an improvement of 92%.
- reducing stator and rotor flux ripples and torque ripples by 40.08%, 29.73%, and 25.88% respectively.
- Acceptable improvements in the THDs of the stator and rotor currents by 37.71% and 21.88% respectively.
- Confirmation of the simulation results extracted from Matlab/Simulink by the experimental validation results extracted from ControlDesk.
- The proved and validated improvements that have been made show the potential efficiency of the proposed strategy in terms of rapidity, precision, and stability of all system performances, confirming the objectives traced previously in the body of the article.

To promote the technical research of our laboratory, our research team has decided to work on the following projects as future work.

- Theoretical studies and experimental validation of the DTC by using ANFIS controllers applied to DFIM.
- Estimation of the DFIM parameters by using artificial intelligence.

CRediT authorship contribution statement

Said Mahfoud: Conceptualization, Software, Validation, Formal analysis, Writing - original draft, Writing - review & editing, Visualization, Funding acquisition. **Aziz Derouich:** Methodology, Validation, Investigation, Resources, Data curation, Writing - review & editing, Supervision, Project administration. **Atif Iqbal:** Writing - review & editing, Supervision, Funding acquisition. **Najib El Ouanjli:** Methodology, Conceptualization, Validation, Writing - review & editing, Funding acquisition.

Declaration of competing interest

The authors declare that they have no known competing financial interests or personal relationships that could have appeared to influence the work reported in this paper.

Acknowledgments

This publication was made possible by Qatar University Collaborative Research grant # [QUCG-CENG-21/22-1] from the

Qatar University. The statements made herein are solely the responsibility of the authors. The APC is funded by the Qatar NAtional Library, Qatar

Appendix

See Tables A.1–A.3.

References

Abderazak, S., Farid, N., 2016. Comparative study between sliding mode controller and fuzzy sliding mode controller in a speed control for doubly fed induction motor. In: 2016 4th International Conference on Control Engineering & Information Technology (CEIT). IEEE, pp. 1–6.

Amezquita-Brooks, L., Liceaga-Castro, E., Liceaga-Castro, J., Ugalde-Loo, C.E., 2015. Flux-torque cross-coupling analysis of FOC schemes: Novel perturbation rejection characteristics. ISA Trans. 58, 446–461.

Ayala, H.V.H., dos Santos Coelho, L., 2012. Tuning of PID controller based on a multiobjective genetic algorithm applied to a robotic manipulator. Expert Syst. Appl. 39 (10), 8968–8974.

Blaschke, F., 1972. The principle of field orientation as applied to the new transvektor closed-loop control system for rotating field machines. Siemens Rev. 34 (1).

BonnetFrancois, F., Vidal, P.E., Pietrzak-David, M., 2007. Dual direct torque control of doubly fed induction machine. IEEE Trans. Ind. Electron. 54 (5), 2482–2490.

Chiha, I., Liouane, N., Borne, P., 2012. Tuning PID controller using multiobjective ant colony optimization. Appl. Comput. Intell. Soft Comput..

Das, K.R., Das, D., Das, J., 2015. Optimal tuning of PID controller using GWO algorithm for speed control in DC motor. In: 2015 International Conference on Soft Computing Techniques and Implementations (ICSCTI). IEEE, pp. 108–112.

Depenbrock, M., 1987. Direct self-control (DSC) of inverter fed induktion machine. In: 1987 IEEE Power Electronics Specialists Conference. IEEE, pp. 632–641.

Devasahayam, V., Veluchamy, M., 2017. An enhanced ACO and PSO based fault identification and rectification approaches for FACTS devices. Int. Trans. Electr. Energy Syst. 27 (8), e2344.

Drid, S., Nait-Said, M.S., Tadjine, M., 2005. Double flux oriented control for the doubly fed induction motor. Electr. Power Compon. Syst. 33 (10), 1081–1095.

El Ouanjli, N., Derouich, A., El Ghzizal, A., Chebabhi, A., Taoussi, M., 2017. A comparative study between FOC and DTC control of the doubly fed induction motor (DFIM). In: 2017 International Conference on Electrical and Information Technologies (ICEIT). IEEE, pp. 1–6.

El Ouanjli, N., Derouich, A., El Ghzizal, A., Chebabhi, A., Taoussi, M., Bossoufi, B., 2018. Direct torque control strategy based on fuzzy logic controller for a doubly fed induction motor. In: IOP Conference Series: Earth and Environmental Science, Vol. 161. IOP Publishing, 012004, (1).

El Ouanjli, N., Derouich, A., El Ghzizal, A., Motahhir, S., Chebabhi, A., El Mourabit, Y., Taoussi, M., 2019a. Modern improvement techniques of direct torque control for induction motor drives-a review. Prot. Control Mod. Power Syst. 4 (1), 1–12.

El Ouanjli, N., Derouich, A., El Ghzizal, A., Taoussi, M., El Mourabit, Y., Mezioui, K., Bossoufi, B., 2019b. Direct torque control of doubly fed induction motor using three-level NPC inverter. Prot. Control Mod. Power Syst. 4 (1), 1–9.

George, M.A., Kamat, D.V., Kurian, C.P., 2021. Electronically tunable ACO based fuzzy FOPID controller for effective speed control of electric vehicle. IEEE Access 9, 73392–73412.

Hasse, K., 1968. Zum dynamischen verhalten der asynchronmaschine bei betrieb mit variabler Standerfrequenz und Standerspannung. ETZ-A Bd 89, 77.

Herlambang, T., Rahmalia, D., Yulianto, T., 2019. Particle swarm optimization (pso) and ant colony optimization (aco) for optimizing pid parameters on autonomous underwater vehicle (auv) control system. J. Phys. Conf. Ser. 1211 (1), 012039, IOP Publishing.

Jayachitra, A., Vinodha, R., 2014. Genetic algorithm based PID controller tuning approach for continuous stirred tank reactor. Adv. Artif. Intell. (16877470).

Kanojiya, R.G., Meshram, P.M., 2012. Optimal tuning of PI controller for speed control of DC motor drive using particle swarm optimization. In: 2012 International Conference on Advances in Power Conversion and Energy Technologies (APCET). IEEE, pp. 1–6.

Krohling, R.A., Rey, J.P., 2001. Design of optimal disturbance rejection PID controllers using genetic algorithms. IEEE Trans. Evol. Comput. 5 (1), 78–82.

Kumar, R., Das, S., Bhaumik, A., 2019. Speed sensorless model predictive current control of doubly-fed induction machine drive using model reference adaptive system. ISA Trans. 86, 215–226.

Madadi, A., Motlagh, M.M., 2014. Optimal control of DC motor using grey wolf optimizer algorithm. Tech. J. Eng. Appl. Sci. 4 (4), 373–379.

Mahfoud, S., Derouich, A., El Ouanjli, N., El Mahfoud, M., Taoussi, M., 2021a. A new strategy-based PID controller optimized by genetic algorithm for DTC of the doubly fed induction motor. Systems 9 (2), 37.

Mahfoud, S., Derouich, A., El Ouanjli, N., Mohammed, T., Hanafi, A., 2021b. Field oriented control of doubly fed induction motor using speed sliding mode controller. In: E3S Web of Conferences, Vol. 229. EDP Sciences, p. 01061.

Mahfoud, S., Derouich, A., Ouanjli, N.E., Taoussi, M., Mahfoud, M.E., 2021c. Improved DTC of the PID controller by using genetic algorithm of a doubly fed induction motor. In: International Conference on Digital Technologies and Applications. Springer, Cham, pp. 1687–1698.

Mazen Alhato, M., Bouallègue, S., Rezk, H., 2020. Modeling and performance improvement of direct power control of doubly-fed induction generator based wind turbine through second-order sliding mode control approach. Mathematics 8 (11), 2012.

Merzoug, M.S., 2008. Etude Comparative des Performances d'Un DTC et d'Un FOC d'Une Machine Synchrone à Aimants Permanents (MSAP) (Doctoral dissertation). Université el Hadj Lakhdar. Faculté des sciences de l'ingénieur), Batna.

Mughees, A., Mohsin, S.A., 2020. Design and control of magnetic levitation system by optimizing fractional order PID controller using ant colony optimization algorithm. IEEE Access 8, 116704-116723.

Nagaraj, B., Murugananth, N., 2010. A comparative study of PID controller tuning using GA, EP, PSO and ACO. In: 2010 International Conference on Communication Control and Computing Technologies. IEEE, pp. 305–313.

Oshaba, A.S., Ali, E.S., Abd Elazim, S.M., 2017. Speed control of SRM supplied by photovoltaic system via ant colony optimization algorithm. Neural Comput. Appl. 28 (2), 365–374.

Ram, S.S., Kumar, C., Madhumitha, J., Nandhini, K.M., 2021. Design and comparison of ACO and fuzzy PID controllers for fermenter system. In: 2021 5th International Conference on Computing Methodologies and Communication (ICCMC). IEEE, pp. 689–694.

Takahashi, I., Noguchi, T., 1997. Take a look back upon the past decade of direct torque control [of induction motors]. In: Proceedings of the IECON'97 23rd International Conference on Industrial Electronics, Control, and Instrumentation (Cat. No. 97CH36066), Vol. 2. IEEE, pp. 546–551.

Takahashi, I., Ohmori, Y., 1989. High-performance direct torque control of an induction motor. IEEE Trans. Ind. Appl. 25 (2), 257–264.

Varol, H.A., Bingul, Z., 2004. A new PID tuning technique using ant algorithm. In: Proceedings of the 2004 American Control Conference, Vol. 3. IEEE, pp. 2154–2159.

Zemmit, A., Messalti, S., Harrag, A., 2018. A new improved DTC of doubly fed induction machine using GA-based PI controller. Ain Shams Eng. J. 9 (4), 1877–1885.